Journal of Sound and Vibration (1999) **225**(3), 527–541
Article No. jsvi.1999.2258, available online at http://www.idealibrary.com on IDEAL®

RADIAL BOUNDARY VIBRATION OF MISALIGNED V-BELT DRIVES

J. MOON

Mechanical Dynamics Incorporated, 2301 *Commonwealth Blvd.*, *Ann Arbor*, *MI*, 48105, *U.S.A.*

AND

J. A. WICKERT

Department of Mechanical Engineering, *Carnegie Mellon University*, *Pittsburgh*, *PA* 15213, *U.S.A.*

(*Received* 26 *August* 1998; *and in final form* 17 *March* 1999)

Mechanical imperfections, including misalignment of the sheaves, can significantly influence the levels of vibration and noise that are produced in power transmission belt drives. In this paper, laboratory measurements identify a particular source of vibration excitation for v-belts that is attributed to lateral misalignment of the sheaves. The belt is shown to undergo a fine, periodic, radial motion on the sheave at a frequency and amplitude that depend on the level of misalignment, the belt's bending stiffness, pre-tension, and wedge angle, the sheave's radius, and the belt-to-sheave friction coefficient, among other modelled variables. Periodic radial oscillation and slippage of the belt in this manner result from frictional stick-slip response at the belt/sheave interface. The belt experiences a prescribed sawtooth-like motion on its boundary, which is one source of its high-frequency vibration and noise. An optical displacement sensor is used to record motion of the belt on the sheave, and those measurements are correlated with the near-field sound pressure. A theoretical model is developed to describe boundary excitation of the belt as is caused by misalignment, and in particular to predict the frequency and amplitude of the boundary motion. The model's predictions are compared with measurements for parameter studies in the belt's pre-tension and in the sheave's radius.

1. INTRODUCTION

V-belts are common machine elements used to transmit torque and/or rotational motion, and they are used in such applications as compressors, appliances, machine tools, and industrial equipment [1–4]. Some important attributes of their design include the mechanical isolation of components from vibration or shock, relatively long working distances between shaft centers, and tolerance of misalignment between drivetrain components. These characteristics stem largely from the belt's compliance and lateral flexibility, which in turn can contribute to vibration of the belt itself.

0022-460X/99/330527 + 15 $30.00/0

Since belt drives employ friction to transmit motion and torque, their load capability is determined by the level at which slippage begins between the belt and its grooved pulley, or sheave. In the most general case, relative motion at the belt/sheave interface comprises two components: one along the sheave's circumference (termed tangential slippage) and the other along its radius (radial slippage). The former limits the drive's torque capacity, with slippage occurring first on the smaller diameter sheave, if any, as the overload condition is reached. Such macroscopic tangential slippage contributes to accelerated wear, fatigue, the production of friction-induced vibration, and squeal noise [5]. The earliest studies of this process were based on a one-dimensional Coulomb model in which the belt's tension varied circumferentially around the sheave. With that approach, Worley [6] established design criteria for belt drives through an extensive empirical and experimental study. Energy loss and failure criteria were later developed for v-belts in terms of the multiple components of stress which act during tangential slippage [7, 8].

Radial slippage also contributes to the belt's vibration and noise, particularly at higher frequencies and in the presence of mechanical misalignment. Such other imperfections as the sheave's geometry, manufacturing variations [9], and load-sharing characteristics [10] are also contributing factors. By way of performance degradation, radial slippage reduces the efficiency of the drive, increases wear, generates noise, and can contribute to eventual fatigue failure [11]. Gerbert [12], and later Dolar and Worley [13], included effects of the belt's radial motion in models of belt/sheave interaction with, and without, tangential slippage being present. In those analyses for sheaves that were well-aligned, the curvature discrepancy between the sheave and the instantaneous configuration of the belt was attributed to radial slippage. Previous investigations have thus emphasized radial slippage from the standpoint of drive performance, but the issues of vibration and noise so produced have received less attention.

In this paper, laboratory experiments identify periodic oscillation of the belt which occurs in the sheave's radial direction and as a result of lateral misalignment. This process is equivalent to boundary excitation of vibration in the belt's free span. The underlying mechanism is stick-slip response at the belt/sheave interface. Periodic slippage of the belt occurs in the presence of misalignment, even without torque overaload, and contributes to the belt's high-frequency response. Measurements correlate the belt's radial oscillation and slippage with periodic bursts in the near-field sound pressure.

A model derived in what follows represents the belt and sheave contact forces at the instant of impending slippage in terms of the level of misalignment, the belt's bending stiffness, pretension, and wedge angle, sheave's radius, and the belt-to-sheave friction coefficient, among other variables that are included in the analysis. The model is used to predict two quantities which describe motion of the belt at its boundary with the sheave: the critical rotation angle of the sheave, and the elevation or rise angle of the belt across its span. Those quantities in turn are related to the frequency and amplitude of boundary excitation. The model's predictions so obtained are compared with measured results for parameter studies in the belt's pre-tension and the sheave's radius.

2. MEASUREMENT OF BELT BOUNDARY MOTION

To guide the model of belt/sheave interaction in the presence of misalignment, laboratory measurements were conducted with the v-belt test stand illustrated in Figure 1. The driven sheave was mounted on an adjustable translation and rotation stage, and it was aligned parallel to the plane of the driver. All other components were rigidly mounted on a vibration isolation table. Different levels d of parallel offset misalignment between the sheaves were set by subsequent adjustment of the fixtures. The conventional commercial v-belt, formed of rubber and having internal reinforcing cords, having span $L_0 = 640$ mm and wedge angle $\beta = 27^\circ$, was driven at velocity v by a variable speed DC motor over drive and idle sheaves of pitch radii $R = 43$, 54, or 85 mm. The belt's pre-tension when the sheaves were well-aligned is denoted by T_0.

A non-contact fiber optic displacement transducer was used to measure motion of the belt as it moved onto the sheave, and a microphone was used to correlate local boundary motion to the sound produced as the belt slipped. The displacement was recorded along the sheave's radial direction, which is equivalent to the direction of the belt's transverse vibration. In order to ensure that sufficient light was reflected from the belt into the sensor's photodiode array, the belt was coated with a thin layer of retroreflective paint. Particles within the paint's matrix ensured that a portion of the incident light was returned into the source optical fiber regardless of the belt's amplitude or slope. Measured displacement and pressure signals were synchronized with the sheave's rotation by using a shaft encoder, and all time records were recorded by a digital oscilliscope and spectrum analyzer.

Measurements of the belt's boundary motion are shown in Figures 2–4 as a function of the sheave's rotation for the lateral misalignment angle $\rho = \tan^{-1}(d/L_0) = 4{\cdot}9^\circ$. This sequence of three figures depicts at increasing levels of resolution the belt's radial motion as it was driven slowly ($v < 0{\cdot}25$ m/s); different ordinate and abscissa scales are used in each figure. Relatively coarse rotation and displacement scales are shown in Figure 2 in order to capture the belt's motion over one complete revolution of the sheave. The transverse motion was periodic with the

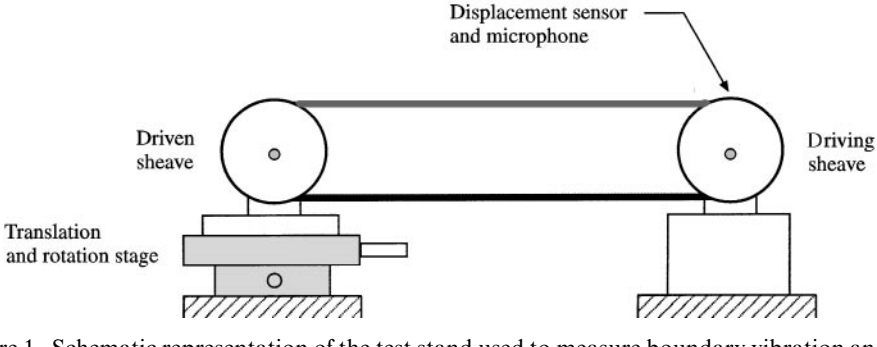

Figure 1. Schematic representation of the test stand used to measure boundary vibration and noise of misaligned v-belts.

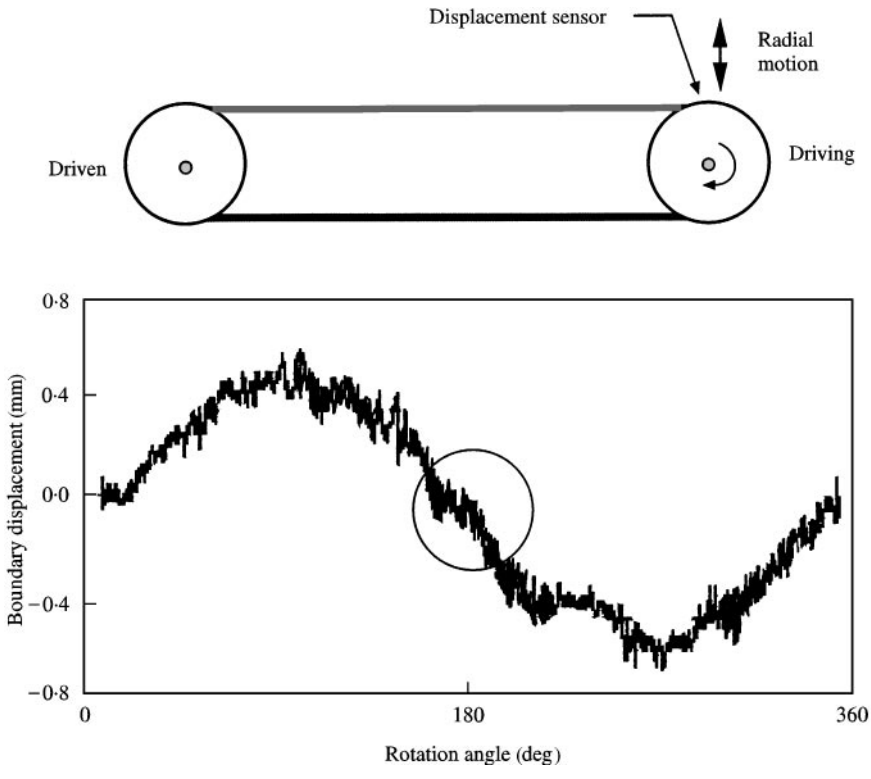

Figure 2. Measured displacement of the belt in the sheave's radial direction, taken at the belt's point of tangency; $\rho = 4{\cdot}9^\circ$, $R = 54$ mm, and $T_0 = 100$ N.

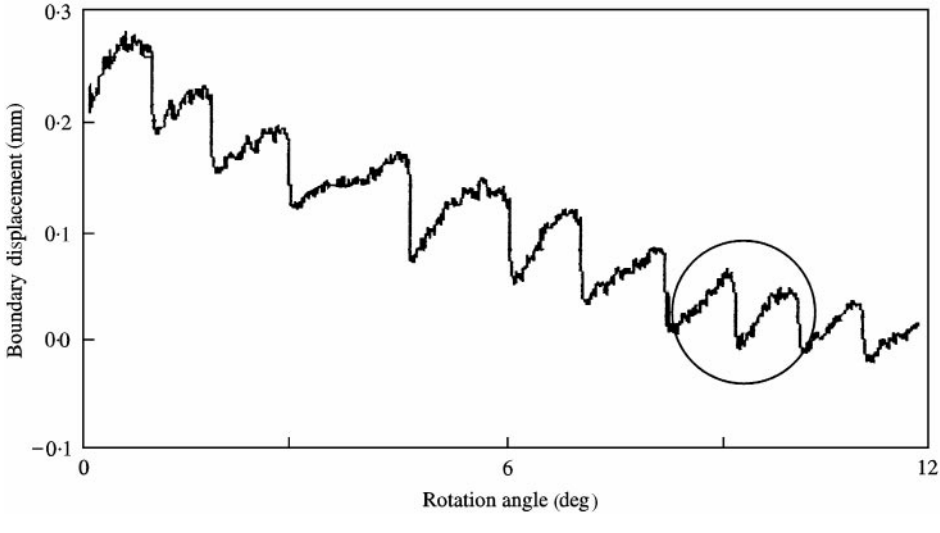

Figure 3. Measured displacement of the belt as in Figure 2; intermediate scale over 12° of rotation.

period being the same as that of the sheave's rotation, and it was dominated by the sheave's eccentricity, essentially independently of misalignment.

A portion of the record in Figure 2 is magnified onto a finer scale in Figure 3. At this level of detail, the measured boundary motion shows the superposition

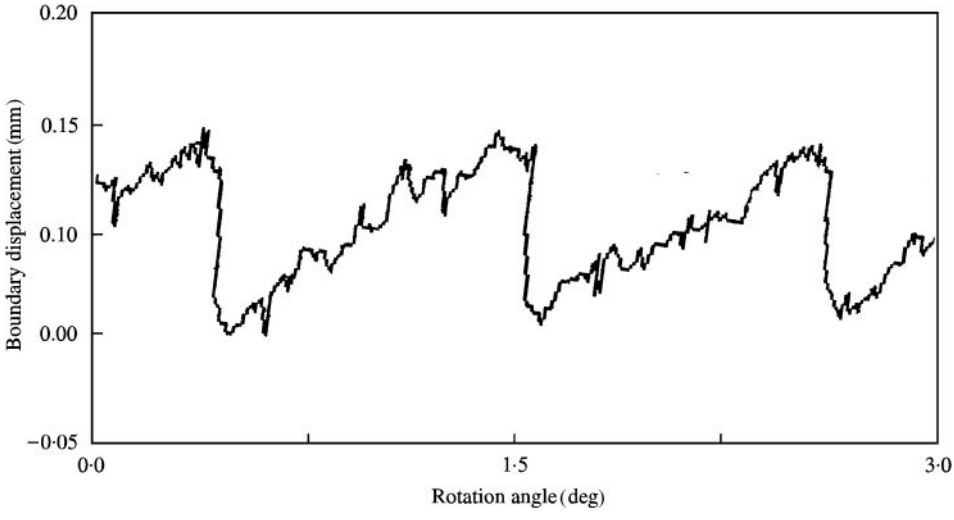

Figure 4. Measured displacement of the belt as in Figures 2 and 3; fine scale over 3° of rotation.

of two effects: (1) motion in the mean which has negative slope and is associated with eccentric mounting of the sheave, and (2) periodic modulation of the eccentricity profile which is attributed to misalignment. The modulation occurred at a substantially higher frequency than the broader eccentricity-induced transverse motion of the belt. At the finest scale of magnification in Figure 4, small-scale transverse motion of the belt is most evident and assumes a sawtooth form. As is characteristic of stick-slip behavior, the belt gradually rose, and then rapidly settled into sheave's groove; the process then repeated itself periodically. In Figure 4, this component of the belt's motion has a peak-to-peak amplitude of approximately 150 μm, and one complete stick-slip cycle occurred as the sheave rotated through roughly 1°.

As is common in phenomena involving friction-vibration interaction, stick-slip motion is often accompanied by the generation of noise. With the belt operating at a transport speed of 2·5 m/s, a sequence of sounds bursts was recorded as shown in Figure 5. One burst occurred for essentially each degree of the sheave's rotation. At this operating speed, the fundamental noise frequency was 1·5 kHz, well within the audible range. The sequence of sound bursts and the corresponding slip motion of the belt were not observed when the sheaves were aligned within the precision of the apparatus. Further, the sound was distinct from that recorded when the belt slipped tangentially as a result of torque overload.

Measurements of radial displacement and sound pressure are synchronized in Figure 6 over a single cycle of response as the sheave was rotated slowly essentially under no load. Motion of the belt within the groove is depicted by the three insets in order to highlight the asymmetry of belt/sheave contact that occurs in the presence of misalignment. In a well-aligned drive, each face of the belt simultaneously contacts a corresponding surface of the sheave such that the belt seats itself fully in the groove. The normal contact loads, which depend on the wedge angle, are distributed evenly in that case. On the other hand, misalignment

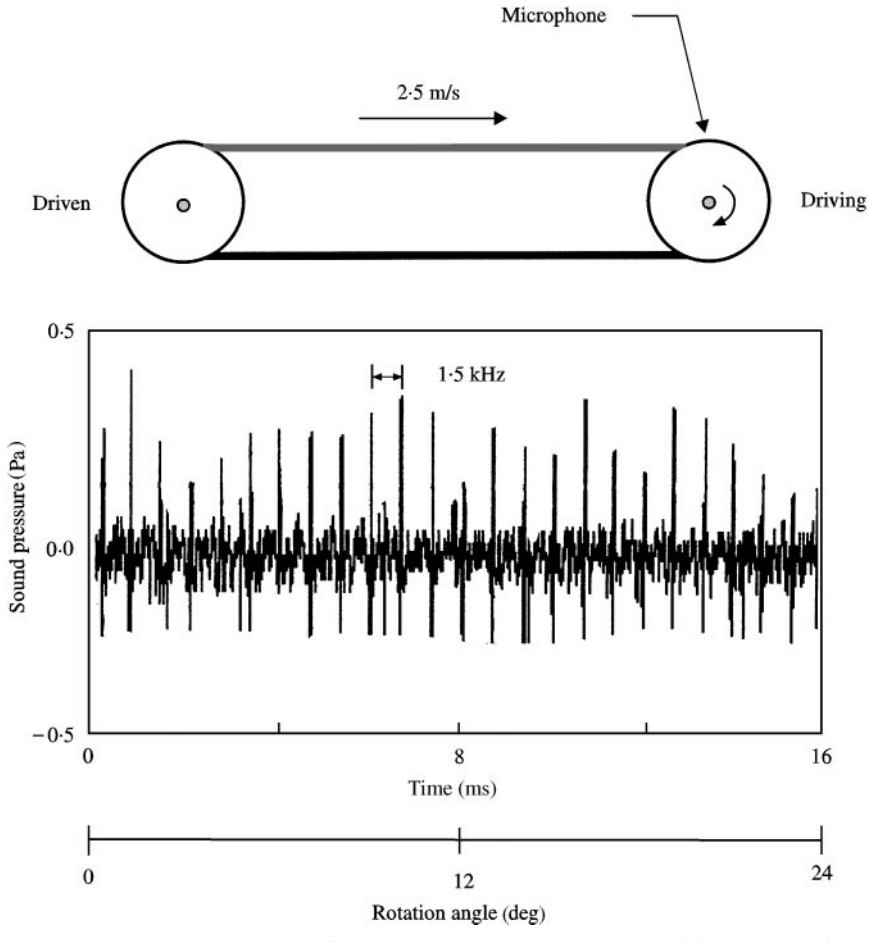

Figure 5. Measured sequence of sound bursts produced at the belt/sheave interface.

generates biased contact against one side of the groove. At the onset of rotation as shown in Figure 6, normal and frictional forces developed between belt and the sheave. With an incremental increase of the rotation angle, the belt was elevated higher within the groove (as in the second loading stage), and it became supported on the left face of the groove under higher normal and friction forces. In the third loading stage, the belt reached its maximum radial elevation δ. The corresponding rotation angle relative to the first loading stage is termed the critical angle α. Under any further rotation of the sheave, the belt rapidly slipped back to its fully seated position, and this sequence repeated itself continuously. The synchronized measurements of Figure 6 demonstrate the radial slippage of the belt correlated with the sound burst, and so the problem fundamentally involves friction- and misalignment-induced vibration.

3. MODEL OF BELT BOUNDARY EXCITATION

The discussed boundary excitation mechanism is characterized by two quantities: α, the critical rotation angle of the sheave at which slippage occurs, and δ, the belt's

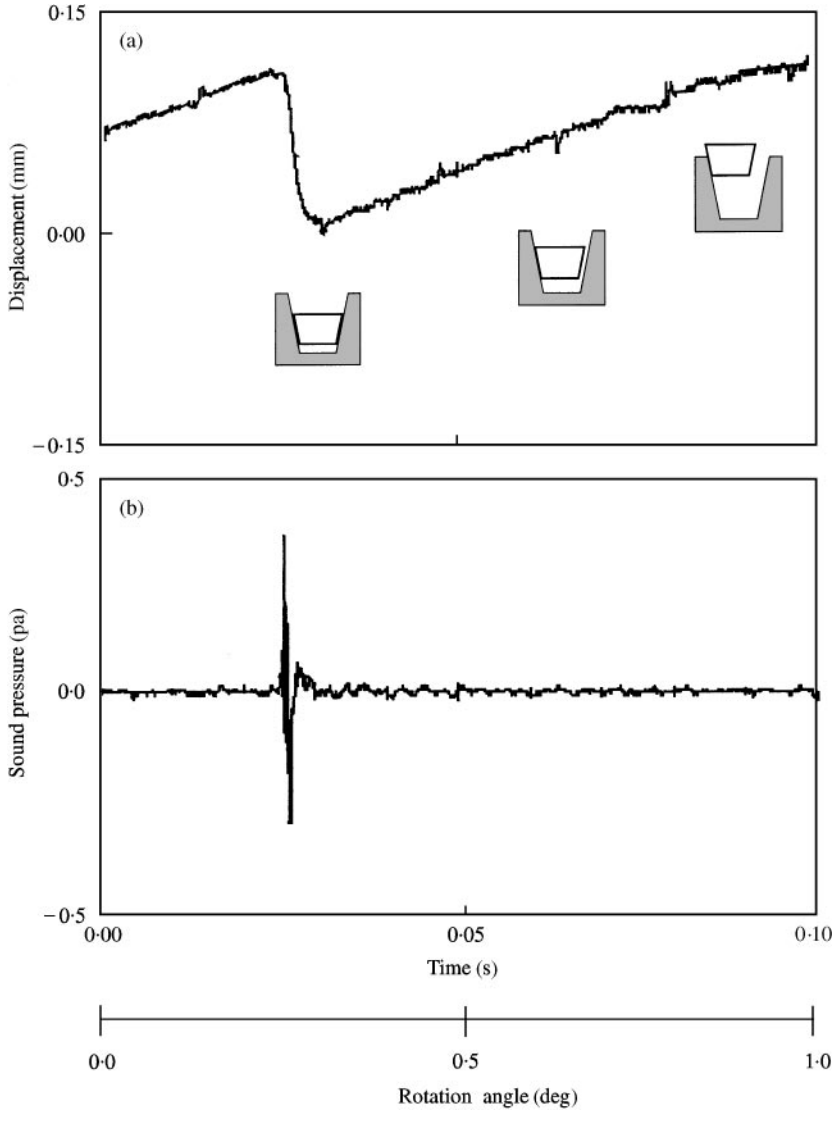

Figure 6. Synchronized measurements of (a) displacement and (b) sound over a single cycle of stick-slip excitation.

rise in elevation. The period of excitation is α/Ω, where $\Omega = v/R$ is the sheave's rotation rate. With those quantities known, the boundary motion of the belt can be represented in the first approximation by a sawtooth-like displacement profile, as shown in Figure 7. In this section, a model is developed to predict α and δ, from which the amplitude and frequency of boundary excitation imposed on the belt can be determined from geometry, the belt's properties, and the drive's operating conditions.

At realistic speeds, the frequency of belt slippage will typically be high when compared with the natural frequencies of the belt's classical transverse vibration

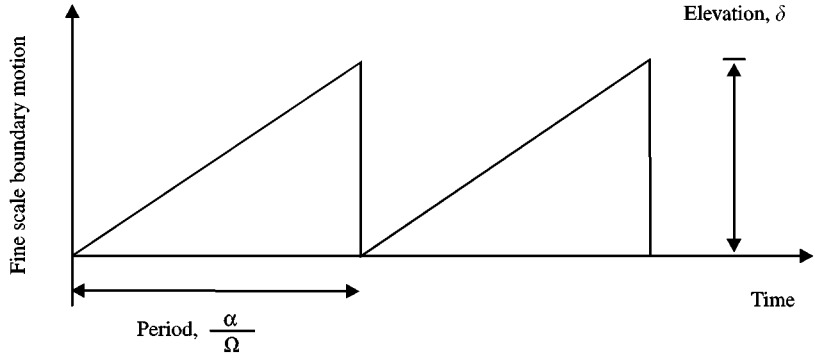

Figure 7. Idealization of the belt's boundary motion in terms of the model's critical angle and elevation rise.

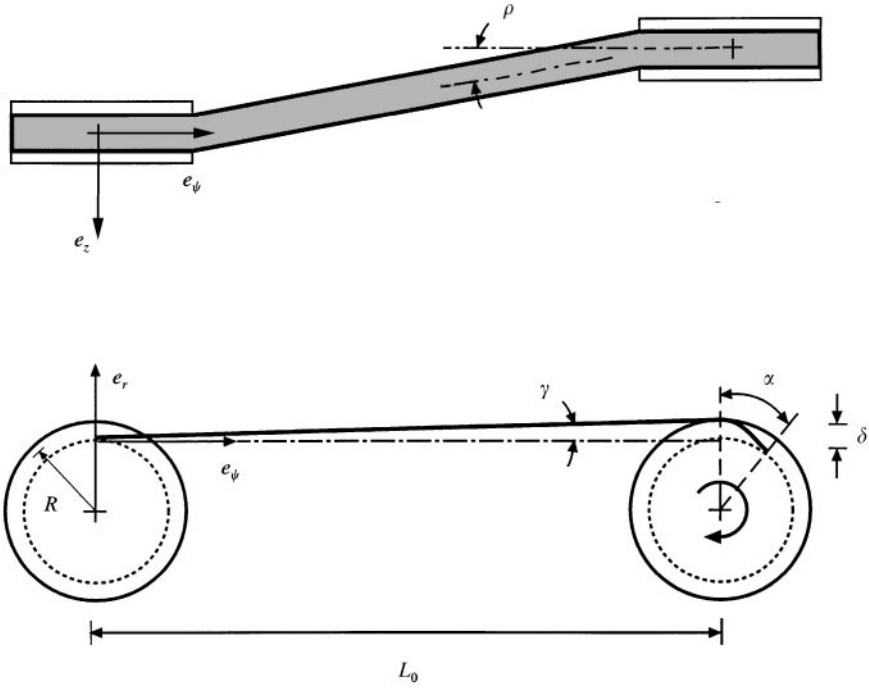

Figure 8. Schematic of a belt drive having sheaves that are offset.

modes. As it enters the sheave, the belt undergoes continuous transition from being straight within the span to conforming with the sheave's circular shape; the instantaneous curvature of the belt is denoted r. This transition region spans angle α and is set by ρ, the elevation angle $\gamma = \tan^{-1}(\delta/L_0)$, and R. As indicated schematically in Figure 8, co-ordinates $(\mathbf{e}_r, \mathbf{e}_\psi, \mathbf{e}_z)$ are used to describe the belt's configuration in the sheave's radial, tangential and normal directions.

The effects of shear and bending within the v-belt become important in balancing the sheave-to-belt contact forces. Those contributions are neglected in analyses of

the contact region in well-aligned drives [12]. The present analytical model for radial slippage and boundary excitation of the belt is developed under the following assumptions. (1) Inertial effects associated with rotation of the sheaves are small when compared to the belt's initial tension. (2) Friction at the onset of slippage is adequately described by the (presumably known) constant coefficient μ. (3) Torsion of the belt and deformation of its cross-section in the $\mathbf{e}_r$–$\mathbf{e}_z$ plane are not significant. (4) Forces acting on the belt's surfaces in the contact zone are uniformly distributed. (5) Beyond the critical angle, the belt follows the circular sheave, as specified in analyses of well-aligned drives.

The three-dimensional forces and moments acting on an element of the belt are illustrated in Figure 9. These components vary with the circumferential co-ordinate ψ. Bending moments M_z and M_r, shear forces V_z and V_r, and tension T act on the element depicted for the instant at which the belt is on the verge of slipping down one face of, and back into, the groove. Resultants P_ψ, P_n, and P_t per unit of belt length act on only one side of the belt, and the other side is force-free because of the asymmetric nature of contact in the presence of misalignment. In the present analysis, the belt is examined at the instant when it rises to peak amplitude on the sheave. At that point, it is on the verge of slipping back into the groove without any further incremental rotation of the sheave, as suggested by Figure 7.

The requirements of force and moment equilibrium provide a system of six equations, in the force and moment components described above and indicated in the diagrams of Figure 9. For instance, $P_t d_1 - P_n d_2 = 0$ is one requirement, where distances d_1 and d_2 are determined from the location of the belt's cross-sectional centroid and the wedge angle. When the belt is on the verge of slippage, the frictional force of magnitude μP_n is resolved into its components P_ψ and P_t acting in the plane of the groove's inclined face. The critical condition for slipping becomes $(\mu P_n)^2 = P_\psi^2 + P_t^2$ from which α and δ can subsequently be determined. In the analysis, this condition is used to determine the critical rotation angle α and elevation angle γ.

Boundary conditions are specified at the point $\psi = 0$ of initial contact with the sheave, and at $\psi = \alpha$, where the belt begins to follow the circular sheave. Moment M_z is determined from the linear moment–curvature relationship, providing the conditions $M_z(0) = -EI_z/(\delta + R)$ and $M_z(\alpha) = -EI_z/R$, where EI_z is the flexural stiffness for bending about $\mathbf{e}_z$. The second set of conditions is provided by the shear force and bending moment in the $\psi - z$ plane, which are approximated at $\psi = 0$ by the known reactions of a beam with offset fixed–fixed ends, namely $V_z(0) = -2EI_r \tan(\rho)/L_0^2$ and $M_r(0) = -6EI_r \tan(\rho)/L_0$. The companion reactions at $\psi = \alpha$ vanish since the belt is supported there fully by the groove, and the variation over angle α is approximated as being linear. For the belt used in the measurements, $d_1 = 4{\cdot}0$ mm, $d_2 = 0{\cdot}25$ mm, $EI_z = 1{\cdot}1\ (10^{-2})\ \mathrm{N\,m^2}$, and $EI_r = 5{\cdot}9\ (10^{-2})\ \mathrm{N\,m^2}$.

Analysis of the coupled force and moment equations provide the expression for the belt's tension,

$$T(\psi) = C_1 e^{\nu\psi} + C_2\psi + C_3, \tag{1}$$

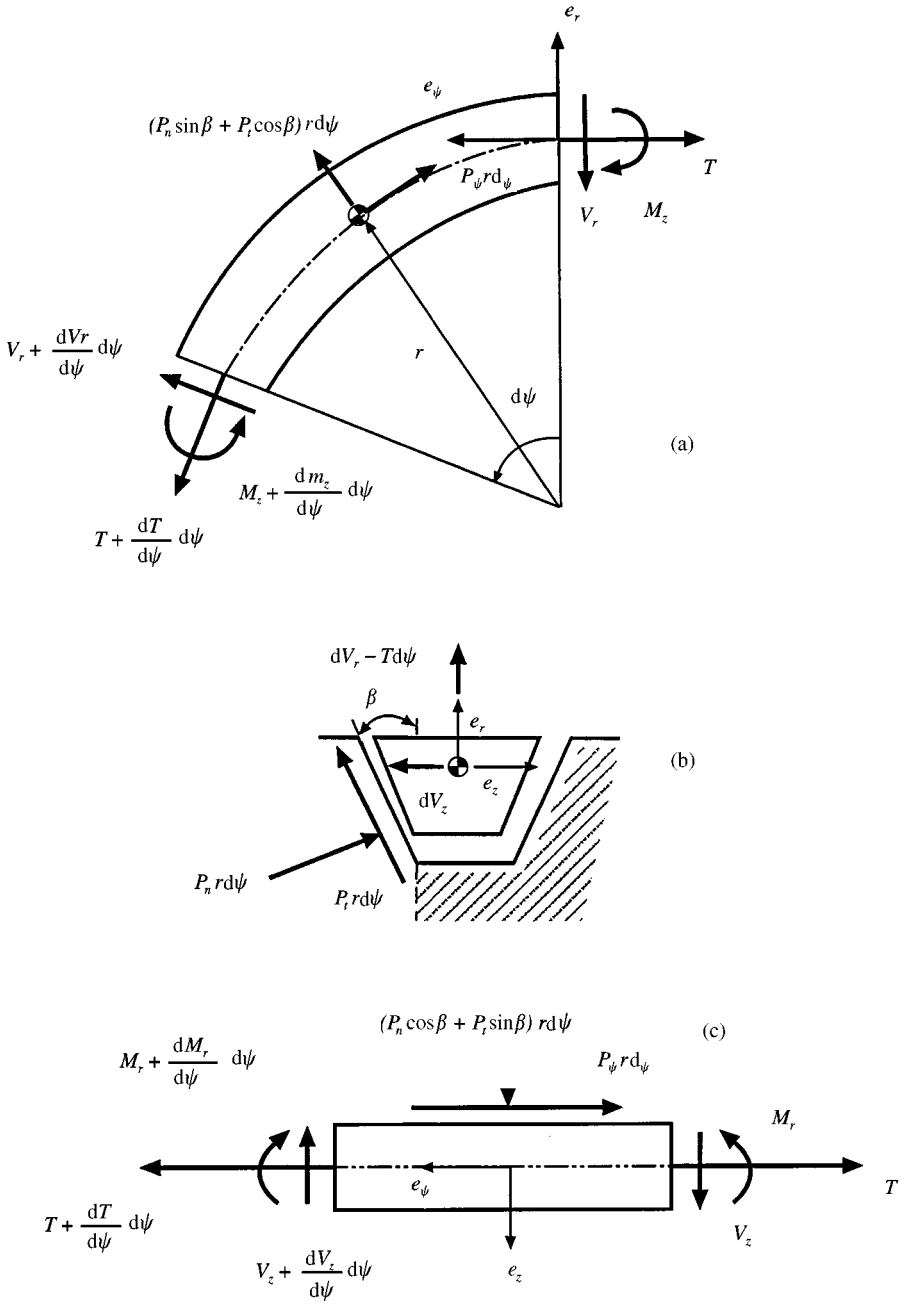

Figure 9. Forces and moments acting on an element of the belt: (a) side view of curved section, (b) cross-section, (c) top view.

where

$$C_1 = T_1 \cos\rho(1 - \gamma(v^2 - v\alpha + 1)/v^2\alpha),\ C_2 = (T_1\gamma/\alpha v)\cos\rho, \qquad (2, 3)$$

$$C_3 = T_1 \gamma \cos\rho(v^2 - v\alpha + 1)/(v^2\alpha),\ v = \frac{\mu\cos\kappa}{\sin\beta + \mu\sin\kappa\cos\beta}. \qquad (4, 5)$$

Here, second order and higher terms in γ have been neglected. When the sheaves are misaligned, the tension rises to $T_1 > T_0$ and is calculated in terms of both the pre-tension and the belt's axial stiffness. That value was $EA = 1{\cdot}2(10^3)$ N for the experimental belt, and typical increases in tension during the tests were on the order of several percent of the initial pre-tension. The friction angle is defined $\kappa = \sin^{-1}(d_1/d_2)$, and it relates P_ψ and P_t at the instant of slipping.

In equation (1), the constant term C_3 arises from the belt's pre-tension and the stretching associated with misalignment, term C_2 is associated with misalignment, and the exponential term C_1 results from the tangential component of friction. Solving for the shear and moment in terms of α and δ and imposing the boundary conditions leads to the non-linear relation for the elevation rise within the groove,

$$\delta = \frac{2EI_r L_0}{\alpha T_1 R^2 \cos^2 \rho} - R\cos\rho = \frac{T_1 \cos(e^{\nu\alpha} - 1)L_0 - 12\nu' EI_z \tan\rho/L_0}{T_1((\nu^2 - \nu\alpha + 1)\nu\alpha/(\nu^2\alpha) - 1/\nu + \alpha/2)}, \quad (6)$$

where

$$\nu' = \frac{\mu\cos\kappa}{\cos\beta - \mu\sin\kappa\sin\beta}. \quad (7)$$

In short, given the model's geometric and material parameters, combinations of α and γ that satisfy equation (6) are determined numerically by using the Newton–Raphson method. Those values are then used to predict the frequency and amplitude of displacement excitation at the belt's boundary with the sheave.

4. DISCUSSION

One input to the model is the friction coefficient between the belt and sheave at the instant of slippage. The appropriate numerical value of μ was determined empirically by monitoring the frequency of radial belt oscillation as a function of speed. With α being independent of speed in principle, the vibration and noise frequency is expected to increase linearly with v. Ten frequency samples were taken and averaged at each of six speeds between 1·5 and 6 m/s as shown in Figure 10. From the known pitch radius of the sheave and the slope of the data, the critical angle $\alpha = 1{\cdot}15^\circ$ was determined from this set of data. When fit to the model, the friction coefficient was estimated as $\mu = 0{\cdot}24$. That value was used in the subsequent calculations of the critical sheave angle and the belt's elevation rise in two parameter studies.

Other experiments indicated that the frequency and amplitude of radial motion were relatively insensitive to ρ when compared with their dependencies on such other model parameters as R and T_0. For that reason, the parameter studies emphasize the behavior of pre-tension and sheave radius on the boundary excitation mechanism.

Figure 11 shows the relationship between the initial pre-tension, α, and δ for both the test results and the model's predictions. At each value of tension, seven measurements such as Figure 4 were made, and the averaged values, as well as the maximum and minimum ones obtained, are shown in Figure 11. Both α and δ

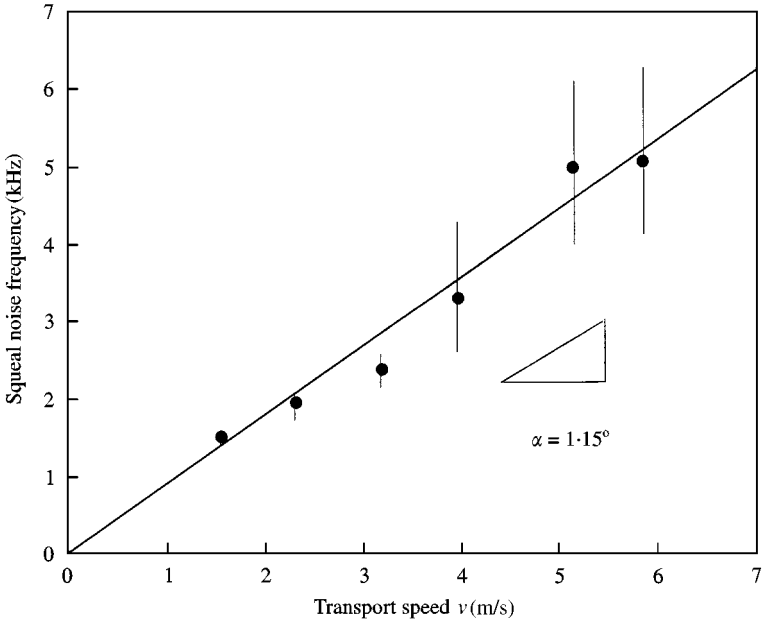

Figure 10. Frequency of noise bursts measured as a function of the belt's transport speed; $\rho = 4{\cdot}9°$, $R = 54$ mm, and $T_0 = 100$ N. Ten measurements were averaged at each speed; ●, average.

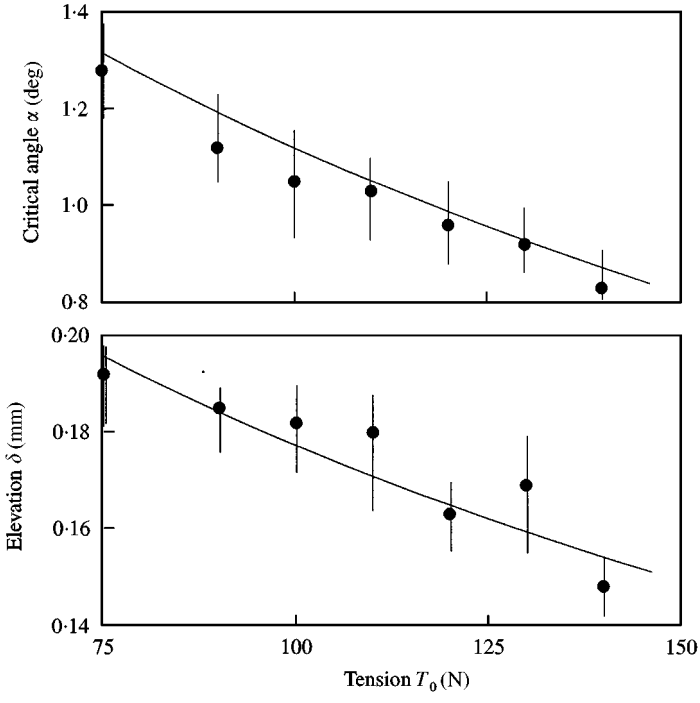

Figure 11. Measured and predicted values of the critical angle and elevation rise as functions of the belt's pre-tension; $\rho = 4{\cdot}9°$, $R = 54$ mm, and $v = 2{\cdot}5$ m/s. Seven samples were averaged at each tension; ●, measured average; ——, predicted.

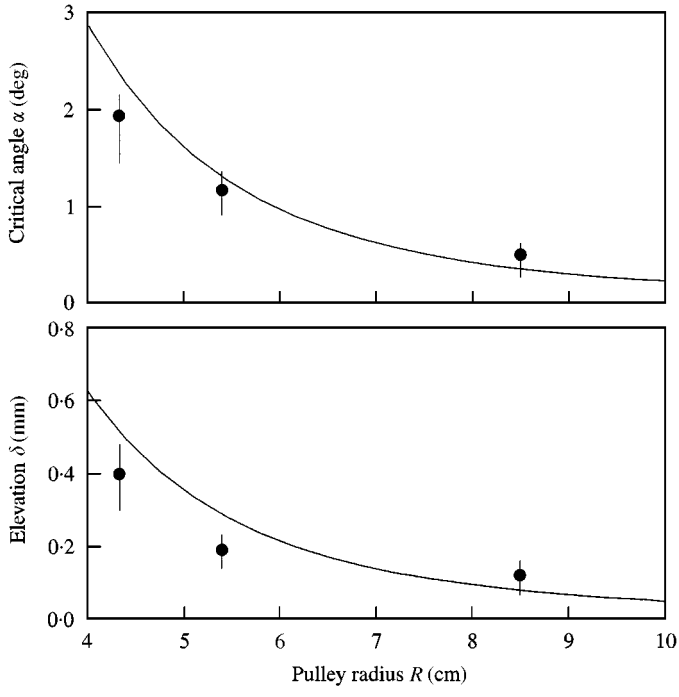

Figure 12. Measured and predicted values of the critical angle and elevation rise as a function of the sheave's radius; $\rho = 4{\cdot}9^\circ$, $T_0 = 100$ N, and $v = 2{\cdot}5$ m/s. Seven samples were averaged at each radius; ●, measured average; ——, predicted.

decrease monotonically by about 25% over the factor-of-two range in pre-tension that was examined, and those values were calculated using the procedure discussed above. The larger T_0 is, the less the belt rises within the sheave, and the higher the frequency of the stick-slip motion.

The effects of sheave size are investigated for three radii in Figure 12. As the radius of the sheave was increased, both the critical angle and elevation decreased measurably. For the belt parameter values used in the case study, the model indicates that beyond a radius of roughly 7 cm, δ and α become insensitive to R. Smaller sheaves generate lower frequency excitation of the belt since α is larger, but the excitation in turn has larger amplitude. This behavior is also noted in Figure 13, where comparisons are made between the time records of noise bursts generated by the three different sheaves. These visual records, taken over identical rotation intervals of 16°, confirm the model's prediction that the frequency is noticeably influenced by the sheave's radius.

5. SUMMARY

Sheave misalignment and other mechanical imperfections can play important roles in determining the vibration and noise of power transmission belt drives. Both eccentricity and misalignment excite motion of the belt on its boundary with the sheave. In the case of eccentricity, the excitation is essentially sinusoidal, and it

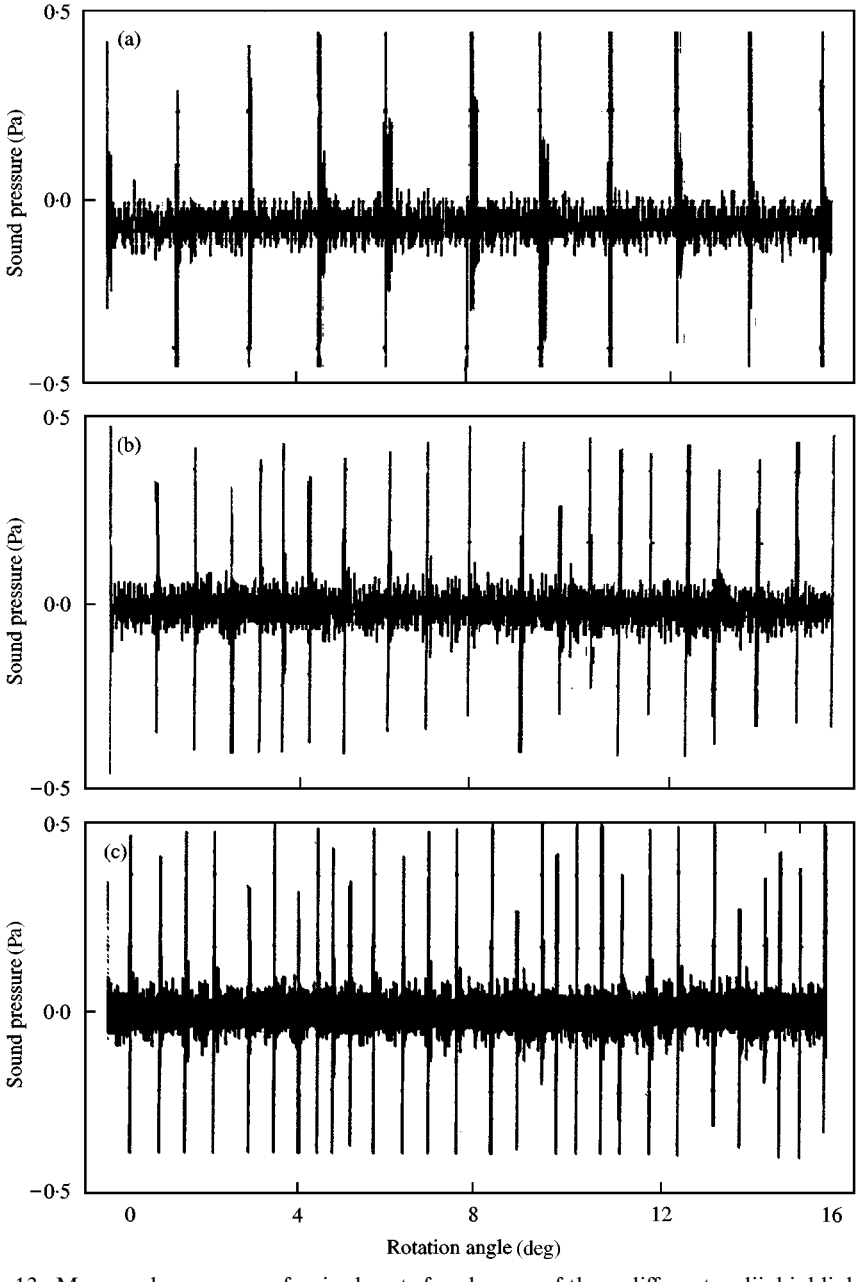

Figure 13. Measured sequences of noise bursts for sheaves of three different radii, highlighting the shift in the frequency of noise generated; $\rho = 4{\cdot}9^\circ$, $T_0 = 100$ N, and $v = 2{\cdot}5$ m/s. (a) $R = 43$ mm and $\alpha = 1{\cdot}9^\circ$; (b) $R = 54$ mm and $\alpha = 1{\cdot}1^\circ$; and (c) $R = 85$ mm and $\alpha = 0{\cdot}6^\circ$.

occurs with rotation of the sheave. Typically, that motion is low enough in frequency to generate substantial structural vibration of the belt [14]. Parallel offset misalignment, on the other hand, produces a sawtooth-like stick-slip motion at a frequency that is determined by the critical angle and operating speed. Periodic

bursts of noise and vibration result, and they are associated with fine-scale slippage of the belt in the groove.

The radial slippage model predicts the critical angle (which is inversely proportional to the frequency of belt excitation) and the elevation rise (which determines the amplitude of boundary excitation imposed on the belt). The results are expected to be useful in noise and vibration analyses of power transmission belt systems, and in understanding the fundamental sources of v-belt vibration.

ACKNOWLEDGMENT

This work was supported by the National Science Foundation and the author's group of industrial partners.

REFERENCES

1. D. C. Sun 1988 *Journal of Mechanisms, Transmissions, and Automation in Design* **110**, 471–481. Performance analysis of a variable speed-ratio metal v-belt drive.
2. H. Kim and J. Lee 1994 *Mechanism and Machine Theory* **29**, 865–876. Analysis of belt behavior and slip characteristics for a metal v-belt CVT.
3. J. E. Shigley and C. R. Mischke 1986 *Standard Handbook of Machine Design*. New York: McGraw-Hill Book Company.
4. L. Gould 1993 *Modern Materials Handling* **43**, 65–69. V-belt drives: common problems and remedies.
5. J. E. Connel and R. L. Rorrer 1992 *Friction-Induced Vibration, Chatter, Squeal, and Chaos*, **ASME DE-49**, 75–85. Friction-induced vibration in ribbed v-belt applications.
6. W. S. Worley 1953 *Product Engineering* **24**, 154–160. Design of v-belt drives for mass produced machines.
7. S. M. Marco, W. L. Starkey and K. G. Hourung 1960 *Journal of Engineering for Industry* **82**, 47–59. A quantitative investigation of the factors which influence the fatigue life of a v-belt.
8. L. R. Oliver, C. O. Johnson and W. F. Brieg 1976 *Journal of Engineering for Industry* **34**, 340–347. V-belt life prediction and power rating.
9. A. S. Abrate 1992 *Mechanism and Machine Theory* **27**, 645–659. Vibration of belts and belt drives.
10. G. Massouros 1989 *Journal of Mechanisms, Transmissions, and Automation in Design* **111**, 153–159. The effect of geometry imperfections on the performance of multiple v-belts drives.
11. O. Luntz 1960 *Konstuktion* **12**, 1–4. Zur theoria des keilscheiben-umschlingungsgetriebes.
12. G. Gerbert 1972 *Acta Polytechnica Scandinavia-Mechanical Engineering Series* **67**, 1–155. Force and slip behavior in v-belt drives.
13. J. P. Dolar and W. S. Worley 1985 *Journal of Mechanisms, Transmissions, and Automation in Design* **107**, 292–300. Closed-form approximations to the solution of v-belt force and slip factor.
14. J. Moon and J. W. Wickert 1997 *Journal of Sound and Vibration* **200**, 419–431. Non-linear vibration of power transmission belts.